GENERAL FRAMEWORK FOR THE DESCRIPTION OF KINETICS OF MUON CATALYZED SYNTHESIS OF HYDROGEN ISOTOPES

By A. Gula*

Joint Institute for Nuclear Research, Dubna, USSR

(Received May 25, 1984)

A general framework is proposed for description of the cycle-by-cycle evolution in time of the processes forming the muon-catalysis chain leading to nuclear synthesis in mixtures of hydrogen isotopes. In the approximation of constant transition rates, practically any μ-atomic and μ-molecular processes can be taken into account and treated strictly. Energy-dependent rates can be also dealt with in an approximate manner. Formulae in which the experimental detection efficiency is taken into account are also presented.

PACS numbers: 25.70.Ij

1. Introduction

With the upsurge of interest in the muon-catalysis of nuclear fusion [1] the need of a comprehensive framework for the description of kinetics of the associated processes becomes evident. Such a framework is primarily necessary to interpret the data which have become [2] or may have soon become available [3] as well as (in an optimist's point of view) for its possible usefulness when the muon-catalyzed nuclear energy production turns out reality [4].

In a classic paper on the subject Gerstein et al. [5] have developed a framework for the description of the "all-cycles" (AC) kinetics of muon-catalyzed fusion in the deuterium/tritium mixture, the case most interesting for the expected (now confirmed) resonance character of the cross section for μ-molecule formation.

In such an approach the appropriate time distributions of fusion events are sums over all cycles initiated by a single muon as it re-enters the chain of processes after being released from a μ-molecule upon catalysing the nuclear synthesis reaction. The (AC)--kinetics has been treated with varying emphases also in Refs. [6–11].

In Ref. [12] the (AC)-kinetics has been considered in detail for one-component media

* Present address: Instytut Fizyki i Techniki Jądrowej AGH, Al. Mickiewicza 30, 30-059 Kraków, Poland.

(pure deuterium or tritium) with the aim of finding optimum conditions for the experimental investigation of the corresponding simple branches of the muon-catalysis graph. Recently, in an advancing degree of completeness of the processes taken into account, the simple-branch kinetics has been extended to the description of the separate cycles in the muon catalysis chain [13–16].

In the present paper we develop a general framework for the cycle-by-cycle description of muon catalyzed nuclear synthesis in arbitrary mixtures of hydrogen isotopes, possibly contaminated by heavier elements. Strict solutions of the kinetic equations are presented in the approximation of constant transition rates. The energy-dependent rates can be also dealt with in an approximate way within the proposed scheme and a manageable computational prescription follows. Creation of μ-atoms and μ-molecules in excited states and the ensuing transitions can be taken into account as well as explicit inclusion of the muon shaking-off from the final state μ-atoms [17] is possible.

The formalism we use is familiar from the theory of signal-flow graphs [18]. However, since very simple graph-theoretical ideas are chiefly involved the formalism is developed in an independent way, mainly to elucidate the specific problems and to introduce a comprehensive notation.

In Section 2 we present the kinetic equations and introduce the associated graphs. The resulting formulae for the time distributions of different objects in the muon-catalysis fusion chain are also written down. Analogous formulae are derived and discussed in Section 3 with inclusion of the experimental registration efficiency. Section 4 contains the discussion of possible extensions of the scheme to incorporate energy-dependent transition rates and to include reversible processes. Concluding remarks end this Section.

2. Kinetic equations

2.1. Kinetic graphs

The processes forming the muon-catalysis chain can be represented by drawing the corresponding kinetic graph. The general structure of such a graph describing k cycles initiated by a single muon is shown in Fig. 1. The graph consists of k identical subgraphs connected to input-output vertices. Each subgraph corresponds to exactly one fusion act catalyzed by the muon. The primary input vertex (μ_{in}) represents the source of muons.

Transitions to the following cycles occur via the muon which is freed after having catalyzed a synthesis reaction (either directly or in a collision of the final state μ-atom with a target center) as well as via the μ-atom (tμ or pμ) produced in the (D+D)μ-fusion. The rightmost vertex (V) in the k-th cycle represents the node for which the solution is sought for.

Fig. 2 shows a more detailed map of the processes in the subgraphs of Fig. 1. The links between the consecutive cycles are shown here as feedback lines (dashed arcs)[1]. The vertices can be grouped in three sets representing: the muon (μ), the μ-atoms (μa) and the μ-molecules (μm). By adding wavy bars we denote "fast" muons and μ-atoms for

[1] As we shall see later, this is a presentation appropriate for the (AC)-kinetics.

which the cross section for creating a μ-atom or μ-molecule, respectively, are negligibly small. The vertices in Fig. 2 have their own structure as indicated in Figs. 3–5. Therefore, the edges of the graphs in Figs. 1 and 2 should be understood as sets of edges connecting the corresponding subgraphs. All output vertices representing the released muon are

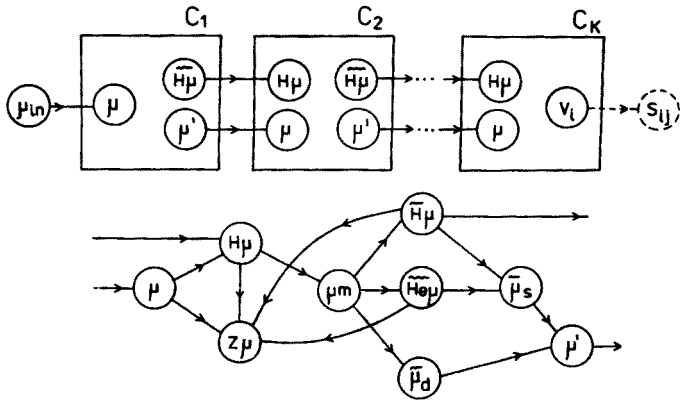

Fig. 1. General structure of the graph representing k cycles of muon-catalyzed fusion chain (top), and general structure of a one-cycle-graph (bottom). Meaning of symbols is explained in text

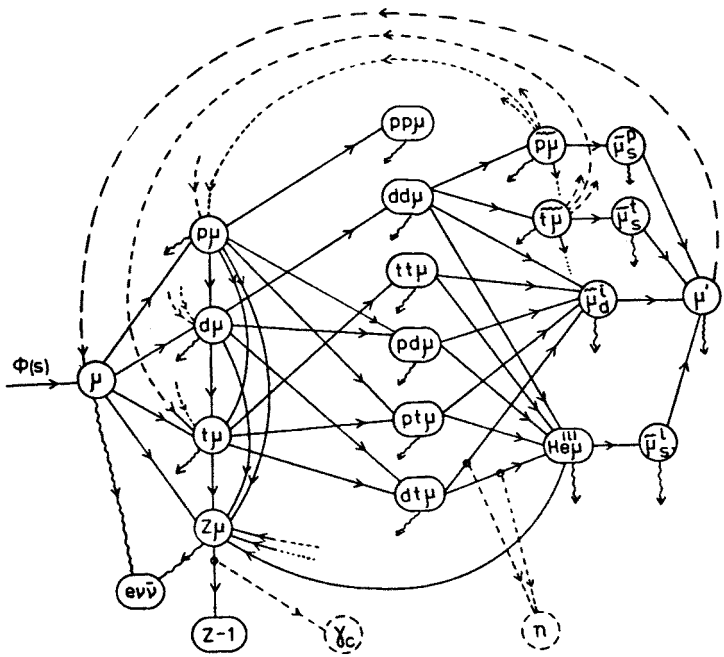

Fig. 2. Kinetic graph representing main μ-atomic and μ-molecular processes leading to muon-catalyzed nuclear fusion in a mixture of H_2, D_2 and T_2 with admixtures of $Z > 1$ elements. Wavy lines indicated at the nodes lead to the ($e\nu\bar{\nu}$) vertex. Other details are described in text

connected to a subsidiary vertex (μ′). This is merely a formal procedure which facilitates the description and, therefore, the content of (μ′) is to some extent arbitrary. For the sake of definiteness we suggest to include in (μ′) muons with energy $E \approx 100$ eV, which is smaller than typical energies of the released muons and still larger than the energies at which muonic atoms are formed [19].

Similarly, for the final-state hydrogen μ-atoms, which can also initiate another cycle, one can assume conveniently that the (Hμ′) nodes in Fig. 3 correspond to energies at which the inverse isotopic exchange transitions become energetically forbidden [20] and the (Hμ)-ones, to thermal energies.

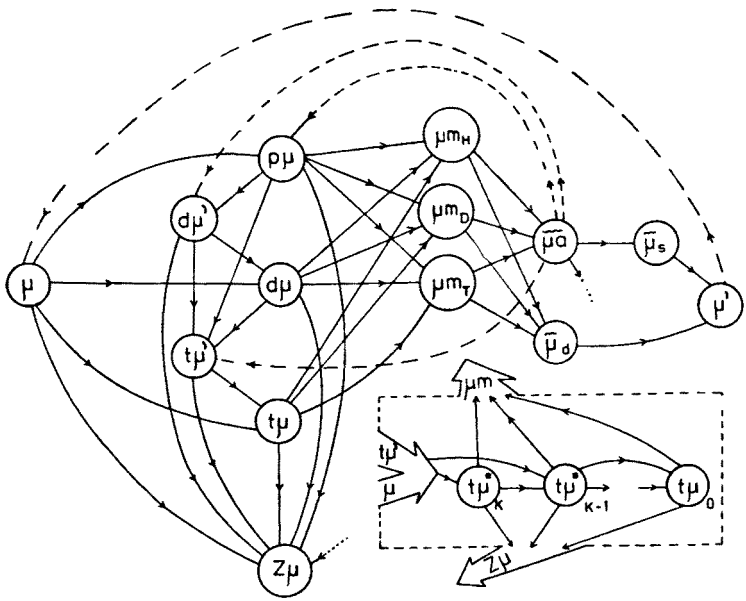

Fig. 3. Graph presenting a more detailed structure of the μ-atomic and μ-molecular vertices in Fig. 2

The μ-molecular nodes of Fig. 2 are split in Fig. 3 into three vertices each: $(\mu m)_H$, $(\mu m)_D$ and $(\mu m)_T$, reflecting the three possibilities of creating the $(^{A_i}H, ^{A_j}H)\mu$-molecule in an $[(^{A_i}H^{A_j}H)\mu, ^{A_k}H,e]^+$ or $[(^{A_i}H, ^{A_j}H)\mu, ^{A_k}H,2e]^*$ molecular compound [1]. The inset in Fig. 3 illustrates the structure of the μ-atomic vertices. Analogous structure for the μ-molecules is shown in Fig. 4 where the nodes represent different vibrational and spin/angular momentum states [20, 21]. Fig. 5 exemplifies fusion in the μ-molecules showing different channels for the (ddμ) node. In Fig. 6 fusion in flight [1, 24, 25] which has been omitted in the previous figures in the interest of keeping the diagrams readable, is additionally included.

Some of the edges of the graphs in Figs. 2–6 correspond to transition rates which are negligibly small (e.g. (dμ) → (dtμ) etc.). We prefer to include them, however, to emphasize the general character of the proposed framework and we leave open the

possibility of the experimental verification of their contributions. If necessary, such transitions can be eliminated by putting the corresponding rates equal to zero.

On the other hand, some processes included in the diagrams are very fast (e.g. $(\mu) \rightarrow (H\mu)$), and may become visible in the data only at very small times [16]. If these are below the experimental resolution the corresponding vertices can be replaced by a single node (e.g., in Fig. 2 all cascade transitions within the $H\mu$-atoms and μ-molecules are contained in single $(H\mu)$ and (μm) vertices). We anticipate that with the advent of high-statistics and high-resolution experiments the choice of vertices to be included explicitly in the kinetic graph will become quite crucial for the description of the data.

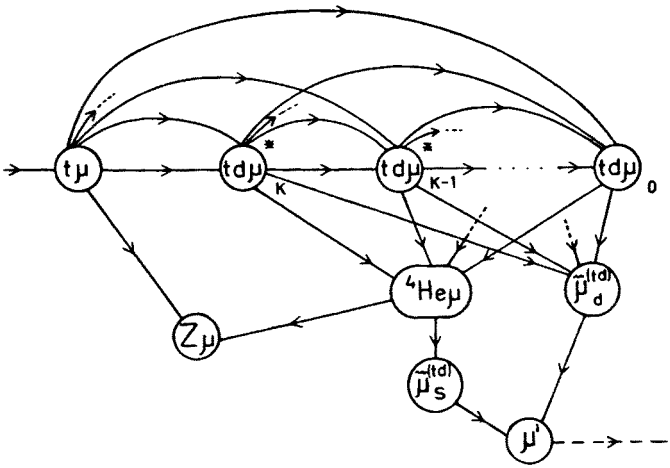

Fig. 4. The structure of the $(td\mu)$ vertex shown to exemplify the structure of the μ-molecular vertices in Fig. 2

In order to secure the overall particle balance in the kinetic graph we introduce in Fig. 2 two common sink vertices (no outgoing lines): $(e\nu\bar{\nu})$ and $(Z-1)$, representing the decay and nuclear capture of the muon, respectively. Below we shall often refer to the one-cycle graph (OCG) which represents a single cycle in the chain. For such graph the following cycle can be, for convenience, considered also as a sink node. Included in the graph of Fig. 2 as examples are also two "signature" vertices (n) and (γ_c). The first one represents the 14 MeV neutrons produced in $d+t \rightarrow {}^4He+n$ [2] and the second one the γ-rays associated with muon capture by a $Z > 1$ nucleus. Similar signature vertices can be associated (at least in principle) with each edge of the kinetic graph. They do not strictly belong to the graph, as they do not contribute to particle balance, but including them in the scheme makes the presentation more transparent and helps to incorporate consistently the experimental registration efficiency in the description of the muon catalysis chain.

The most important topological feature of the kinetic graph is absence of links between different cycles other than via the (μ') and $(\widehat{H\mu})$ exit nodes. Other features are: absence

[2] E.g. we consider the outgoing neutron as a signature of the fusion act in the $dt\mu$-molecule.

of $(\mu) \rightarrow (\mu m)$, $(\widehat{\mu a})$, $(\widehat{\mu})$, (μ') and $(H\mu) \rightarrow (\widehat{\mu a})$, $(\widehat{\mu})$, (μ') edges as well as absence of links between different μ-molecules, and molecular compounds of Figs 2 and 3. Additionally, only one-way links exist between most of the vertices. In fact, in Figs. 1–5 only such links are admitted which means, in particular, that there are no closed loops in the OCG.

Indeed, reversible processes may occur only within the μ-atomic nodes. The isotope exchange transitions (e.g. $(d\mu) \rightarrow (t\mu)$) are irreversible, at least, up to corrections due to the high-energy tail of the Maxwell distribution. In practice, in the temperature range of interest ($T \lesssim 10^3$ K) important reversible transitions may arise only between the closely separated hyperfine structure states of dμ atoms ($\Delta E_{hfs} = 0.049$ eV [20]). Inclusion of

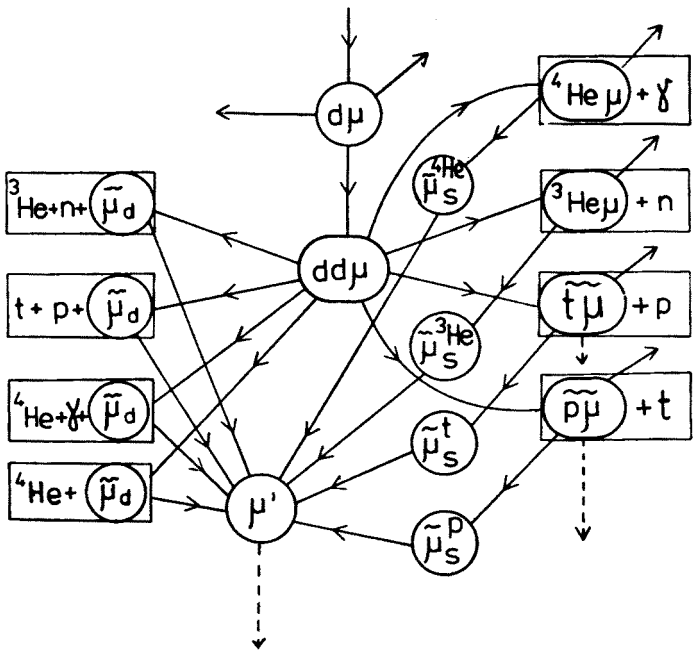

Fig. 5. Graph showing different fusion channels for the ddμ-molecule. Dashes lines indicate feedback lines of Fig. 2. Arrows at the μ-atomic vertices represent transitions to $(Z\mu)$

reverse links poses no fundamental difficulty. However, appearance of closed loops within OCG makes the simple one-link formalism slightly more involved. Therefore, in the interest of simplifying the presentation, we postpone the discussion of the reversible transitions till the final Section.

2.2. Kinetic equations

Let us follow the history of the muon up to the k-th cycle. The equations describing the numbers of particles in the nodes of the kinetic graph are then:

$$\frac{dN_\mu^{(1)}}{dt} = -\Lambda_\mu N_\mu^{(1)}(t) + \frac{d\phi(t)}{dt},$$

$$\cdots\cdots\cdots\cdots$$

$$\frac{dN_{n_\nu}^{(1)}}{dt} = -\Lambda_{n_\nu} N_{n_\nu}^{(1)}(t) + \sum_j \lambda_{n_\nu j} N_j^{(1)}(t),$$

$$\frac{dN_{\mu}^{(2)}}{dt} = -\Lambda_{\mu} N_{\mu}^{(2)}(t) + \lambda_{\mu\mu'} N_{\mu'}^{(1)}(t),$$

$$\frac{dN_{p\mu}^{(2)}}{dt} = -\Lambda_{p\mu} N_{p\mu}^{(2)} + \lambda_{p\mu,\mu} N_{\mu}^{(2)} + \sum_{\widetilde{H\mu}} \lambda_{p\mu,\widetilde{H\mu}} N_{\widetilde{H\mu}}^{(1)},$$

$$\frac{dN_{d\mu'}^{(2)}}{dt} = -\Lambda_{d\mu'} N_{d\mu'}^{(2)} + \lambda_{d\mu',p\mu} N_{p\mu}^{(2)} + \sum_{\widetilde{H\mu}} \lambda_{d\mu',\widetilde{H\mu}} N_{\widetilde{H\mu}}^{(1)},$$

$$\cdots\cdots\cdots\cdots$$

$$\cdots\cdots\cdots\cdots$$

$$\frac{dN_l^{(\nu)}}{dt} = -\Lambda_l N_l^{(\nu)} + \sum_j \lambda_{lj} N_j^{(\nu)} + \sum_{m=\mu',\widetilde{H\mu}} \lambda_{l,m} N_m^{(\nu-1)},$$

$$\cdots\cdots\cdots\cdots$$

$$\cdots\cdots\cdots\cdots$$

$$\frac{dN_{n_\nu}^{(k)}}{dt} = -\Lambda_{n_\nu} N_{n_\nu}^{(k)} + \sum_j \lambda_{n_\nu, j} N_j^{(k)}, \tag{1}$$

where n_ν is the number of vertices in a one-cycle graph, λ_{lj} are transition rates from the j-th to l-th vertex and

$$\Lambda_l = \sum_{\substack{i \\ \text{all lines leaving} \\ \text{vertex } (l)}} \lambda_{il}. \tag{2}$$

$N_l^{(\nu)}(t)$ is the number of particles in the l-th node of the ν-th cycle and $\phi(t)$ represents the muon source. In writing down Eqs. (1) we have exemplified the equations for the inter-cycle transitions using the topology of the graph in Fig. 3.

After taking the Laplace transforms of Eqs. (1) one obtains a set of algebraic equations for the transformed functions:

$$N_l^{(\nu)}(s) = \int_0^\infty e^{-st} N_l^{(\nu)}(t) dt \tag{3}$$

which can be conveniently written as

$$\hat{A}(s)\vec{N}(s) = \vec{I}(s) \tag{4}$$

with $\vec{N}(s) = [N_\mu^{(1)}(s), \ldots N_{n_\nu}^{(k)}(s)]^T$ and with matrix $\hat{A}(s)$ having the following structure:

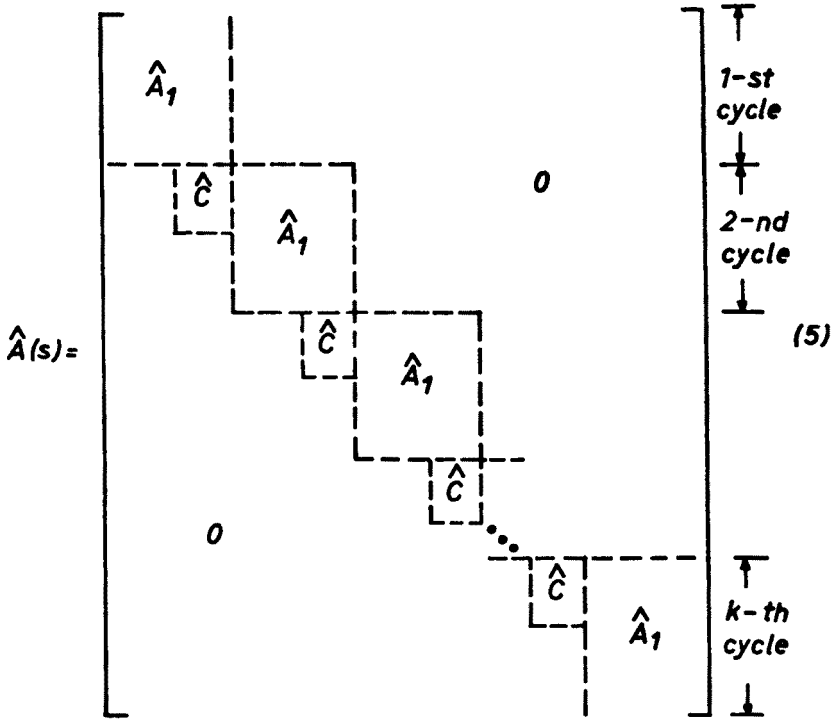

The off-diagonal matrix $\hat{C}$ links the neighbouring cycles and $\hat{A}_1$ defines the one-cycle graph of Figs. 1–5. If the equations are ordered so that in $\vec{N}(s)$ only transitions from higher to lower $N_i^{(\nu)}(s)$ are possible (temporarily we admit only one-way links), one has:

$$\hat{A}_1(s) = \begin{bmatrix} 1 & & & \\ & 1 & & 0 \\ & & 1 & \\ & -\frac{\lambda_{ij}}{\Lambda_i+s} & & 1 \end{bmatrix}. \qquad (6)$$

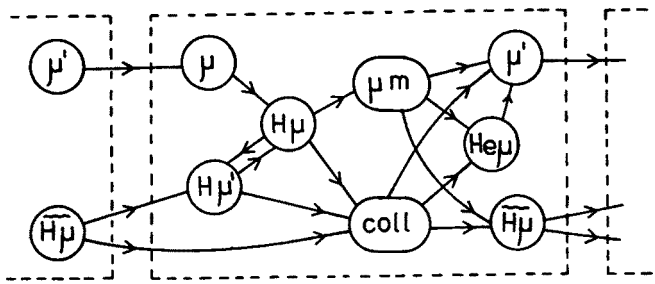

Fig. 6. General structure of one-cycle-graph with fusion in flight taken into account. The vertex denoted by (coll) is a subsidiary vertex representing the nuclear interaction without creation of the μ-molecule

Then

$$\det \hat{A}(s) = \det \hat{A}_1(s) \equiv 1. \tag{7}$$

The unit entries in the diagonal arise after dividing each transformed equation (1) by the coefficient at the LHS function $N_l^{(\nu)}(s) : (\Lambda_l + s)$. Thus, in accordance with Figs. 1, 2:

$$\hat{C}(s) = \begin{bmatrix} 0, & 0, & -\frac{\lambda_{\mu\mu'}}{\Lambda_\mu + s} \\ -\frac{\lambda_{p\mu,\widetilde{t\mu}}}{\Lambda_{p\mu}+s}, & -\frac{\lambda_{p\mu,\widetilde{p\mu}}}{\Lambda_{p\mu}+s}, & 0 \\ -\frac{\lambda_{d\mu,\widetilde{t\mu}}}{\Lambda_{d\mu}+s}, & -\frac{\lambda_{d\mu,\widetilde{p\mu}}}{\Lambda_{d\mu}+s}, & 0 \\ -\frac{\lambda_{t\mu,\widetilde{t\mu}}}{\Lambda_{t\mu}+s}, & -\frac{\lambda_{t\mu,\widetilde{p\mu}}}{\Lambda_{t\mu}+s}, & 0 \end{bmatrix} \tag{8}$$

If fusion in flight (Fig. 6) is taken into account, the number of rows in $\hat{C}$ will correspondingly increase. The vector describing input into the chain is

$$\vec{I}(s) = \left[\frac{s\phi(s)}{\Lambda_\mu + s}, 0, 0, \ldots 0\right]^T. \tag{9}$$

Let us remark that in our notation the muon sticking coefficients, ω_i, and fusion channel branching ratios, b_i, are included in λ_{ij}. E.g., referring to the conventional notation:

$$\lambda_{\widetilde{t\mu},dd\mu} = \lambda_{dd\mu}^{(f)} b_t \omega_{t\mu}. \tag{10a}$$

For transition rates which are determined by collision cross sections

$$\lambda_{ij} = n_i \sigma_{ij}^{(i)} v_j \tag{10b}$$

also included in λ_{ij} are: relative concentration, c_i, of the respective target centers and the overall target density, $\varphi = n/n_0$ (n_0 is usually assumed to correspond to liquid hydrogen density: $4.25 \cdot 10^{22}\,\mathrm{cm}^{-3}$).

By inspection of the matrix $\hat{A}(s)$ one can easily find the solution for any node (l) in an arbitrary k-th cycle:

$$\vec{N}^{(k)}(s) = \hat{T}_f(\hat{C}\hat{T})^{k-1}\vec{I}_1(s), \tag{11}$$

where $\hat{T}_f(s)$ is a $(n_v \times n_{in})$ matrix the entries of which are

$$\{\hat{T}_f(s)\}_{li} = (-1)^{l+i} M_{il}(s), \tag{12}$$

$M_{il}(s)$ are minors of $\hat{A}_1$ corresponding to the i-th row and l-th column, n_v and n_{in} denote the number of all vertices and the number of input vertices in the one-cycle graph, respectively, index l running over all OCG nodes and i over all input ones. Analogously, $\hat{T}(s)$ is

a $(n_{out} \times n_{in})$ matrix with elements defined by Eq. (12), the first index running now over all exit nodes of OCG: 1, ..., n_{out}. $\vec{I}_1(s)$ is given by Eq. (9), being now a n_{in}-dimensional vector representing input to the first cycle.

It is convenient to consider Eq. (11) as a result of an iterative procedure of constructing $\vec{N}^{(k)}(s) = [N_1^{(k)}(s), \ldots N_{n_v}^{(k)}(s)]^T$

$$\vec{N}^{(k)} = \hat{T}_f \vec{I}_k = \hat{T}_f \hat{C} \vec{W}_{k-1} = \hat{T}_f \hat{C} \hat{T} \vec{I}_{k-1} = \ldots = \hat{T}_f (\hat{C}\hat{T})^{k-1} \vec{I}_1 \tag{13}$$

where $\vec{I}_\nu = \vec{I}_\nu(s)$ represents an input to the ν-th cycle and $\vec{W}_\nu = \vec{W}_\nu(s)$ the set of the resulting solutions for the exit vertices of the same cycle.

Yet another way of viewing the solutions for $\vec{N}^{(k)}(s)$ follows from the graph-theoretical interpretation of Eq. (11). Namely, the solution for $N_l^{(k)}(s)$ is a sum of terms:

$$g_m(s) = \frac{\lambda_{l l'}}{\Lambda_l + s} \cdot \frac{\lambda_{l' l''}}{\Lambda_{l'} + s} \cdots \frac{\lambda_{2\mu}}{\Lambda_2 + s} \cdot \frac{s\phi(s)}{\Lambda_\mu + s}, \tag{14}$$

where the set $\{\lambda_{ll'}, \lambda_{l'l''}, \ldots \lambda_{2\mu}\}$ can be associated with an m-th "forward path" from (μ_{in}) to $(l)_k$, which is a sequence of forward directed edges, one following another, leading from the primary input vertex (μ_{in}) to the vertex (l) in the k-th cycle [18]. Thus[3]

$$N_l^{(k)}(s) = \frac{s\phi(s)}{\Lambda_\mu + s} \sum_{\substack{\text{all forward} \\ \text{paths} \\ (\mu)_1 \to (l)_k}} \prod_{\substack{m\text{-th} \\ \text{forward} \\ \text{path}}} \left(\frac{\lambda_{ij}}{\Lambda_i + s} \right). \tag{15}$$

Therefore, the solutions for $N_l^{(k)}(s)$ can be found either by direct application of Eq. (11) or by inspection of the kinetic graph.

A general structure of $N_l^{(k)}(s)$ is:

$$N_l^{(k)}(s) = s\phi(s) \sum_{\substack{\text{all forward} \\ \text{paths } (\mu)_1 \to (l)_k}} \frac{\prod_{\text{OCG edges}} \lambda_{ij}^{\kappa_{ij}}}{\prod_{\text{OCG nodes}} (\Lambda_n + s)^{r_n}}, \tag{16}$$

where κ_{ij} and r_n are multiplicities of λ_{ij} and $(\Lambda_n + s)$ in the forward path, respectively, and $\Sigma r_n = \Sigma \kappa_{ij} + 1$.

Analogously, the time distributions of signatures associated with the vertex (l) in the k-th cycle

$$\frac{dS_l^{(k)}}{dt} = \lambda_l^{reg} N_l^{(k)}(t), \tag{17}$$

---

[3] It is easy to check that for the matrix $\hat{A}$ given by Eqs. (5)–(8) all terms in (15) are positive, as should be expected from the physical interpretation. The terms in (15) are often referred to as path transmissions or path products [18].

where λ_l^{reg} is a sum over the registered transitions

$$\lambda_l^{reg} = \sum_{\substack{\text{registered} \\ \text{transitions} \\ (l)\to(j)}} \lambda_{jl} \tag{18}$$

is given by

$$sS_l^{(k)}(s) = \lambda_l^{reg} N_l^{(k)}(s). \tag{19}$$

The total yield of signatures defined by Eqs. (17), (18) follows immediately from (16) and (19):

$$Y_l^{(k)} = \int_0^\infty \frac{dS_l^{(k)}}{dt}\, dt = \lambda_l^{reg} \sum_{\substack{\text{f.p.} \\ (\mu)_1\to(l)_k}} \frac{\prod \lambda_{ij}^{\kappa_{ij}}}{\prod \Lambda_n^{r_n}} [s\phi(s)]_{s=0}. \tag{20}$$

If we choose $\phi(t)$ to represent a single muon which enters the chain at $t = 0$ ($\phi(t) = 0$ for $t < 0$, $\phi(t) = 1$ for $t \geqslant 0$):

$$s\phi(s) \equiv 1, \tag{21}$$

the time distribution (17) which is the inverse Laplace transform of (19) is given by a direct generalization of the formulae of Ref. [16]:

$$\frac{dS_l^{(k)}}{dt} = \lambda_l^{reg} \sum_{\substack{\text{all f.p.} \\ (\mu)_1\to(l)_k}} \frac{\prod_{\text{f.p. OCG edges}} \lambda_{im}^{\kappa_{im}}}{\prod_{\text{f.p. OCG nodes}} (r_n-1)!} \sum_{\substack{\Lambda_j \\ \text{in f.p.}}} e^{-\Lambda_j t}$$

$$\times \sum_{p=1}^{r_j} \binom{r_j-1}{p-1} t^{r_j-p} \sum_{\{q_1\dots q_s\dots q_{n_\nu}\}, s\neq j} (-1)^{p-1} \binom{p-1}{q_1 \dots q_s \dots q_{n_\nu}} \prod_{\substack{\text{f.p.OCG} \\ \text{nodes}\neq(j)}} \frac{(r_n-1+q_n)!}{(\Lambda_n-\Lambda_j)^{r_n+q_n}}. \tag{22}$$

Before proceeding further let us consider Eq. (11) for the particular case where only one feedback line: $(\mu') \to (\mu)$ is taken into account. Then:

$$\hat{C}\hat{T} \to G(s) = \frac{\lambda_{\mu\mu'}}{(\Lambda_\mu+s)} |M_{\mu\mu'}(s)|, \tag{23}$$

where

$$|M_{\mu\mu'}(s)| = \sum \frac{\lambda_{\mu'\tilde{\mu}}}{(\Lambda_{\mu'}+s)} |M_{\mu\mu';\mu'\tilde{\mu}}(s)| \tag{24}$$

and the summation goes over all lines contributing to (μ'). When $(\tilde{\mu}_d^{(i)})$ and $(\tilde{\mu}_s^{(i)})$ are replaced by common vertices $(\tilde{\mu}^{(i)})$ describing the muons released in the i-th fusion channel one obtains:

$$G(s) = \frac{\lambda_{\mu\mu'}}{(\Lambda_\mu+s)(\Lambda_{\mu'}+s)} \sum_{\substack{(\mu m), \\ \text{channels}}} \lambda_{\mu m}^{(f)} b_l^{(\mu m)} (1-\bar{\omega}_i^{(\mu m)}) |M_{\mu\mu';\mu'\tilde{\mu}_l)}| \tag{25}$$

where $\bar{\omega}_i$ are "effective" sticking coefficients corrected for muon shaking-off [17].

In particular, for the one-dimensional chains (fusion in pure D_2 or T_2 targets can be so approximated) Eqs. (23) and (25) give the formulae obtained in Ref. [16].

2.3. All-cycles equations

When the number of particles in each node is summed over all cycles the resulting equations for

$$\vec{N}^{(AC)}(s) = \sum_{k=1}^{\infty} \vec{N}^{(k)}(s) \tag{26a}$$

are

$$\hat{A}^{(AC)}(s)\vec{N}^{(AC)}(s) = \vec{I}(s) \tag{26b}$$

with $\hat{A}^{(AC)}(s)$ being a $(n_v \times n_v)$ matrix:

$$\hat{A}^{(AC)}(s) = \begin{bmatrix} 1 & & 0 & \hat{C}(s) \\ & 1 & & 0 \\ & & \ddots & \\ -\frac{\lambda_{lj}}{\Lambda_l + s} & & 1 & \\ & & & 1 \end{bmatrix} \tag{27}$$

Now, in general,

$$\det \hat{A}^{(AC)}(s) = \Delta(s) \neq 1. \tag{28}$$

The procedure of finding $\vec{N}^{(AC)}(s)$ is straightforward, although writing down all contributing terms may become involved. Therefore, it seems reasonable to indicate here a possibility of constructing $\vec{N}^{(AC)}(s)$ by inspection of the (AC)-kinetic graph (ACG) which is the one-cycle graph (OCG) with the feedback lines included.

According to Mason's topological formula [22, 18] the solution can be found by enumerating all closed loops in the graph (all edge orientations in the loop have to agree) and grouping them into vertex-disjoint sets, i.e., sets of loop having no common vertices. Then[4]

$$N_l^{(AC)}(s) = \sum_{\substack{\text{all f.p.} \\ (\mu)\to(l) \\ \text{in ACG}}} \frac{g_k(s)\Delta_k(s)}{\Delta(s)}, \tag{29}$$

where $g_k(s)$ are transmissions (14) for the k-th forward path in the ACG[5],

$$\Delta(s) = 1 - \sum P_{m1} + \sum P_{m2} - \sum P_{m3} \cdots \tag{30}$$

---

[4] Notation of Ref. [18] is followed.

[5] Note that if ACG contains more than one feedback line there are more forward paths $(\mu) \to (l)$ in ACG than in OCG. For example: $(\mu) \to (\mu m) \to (\widehat{H\mu}) \to (H\mu) \to (l)$ is a forward path in ACG if none of the vertices is traversed twice.

P_{m1} are products of $\lambda_{ij}/(\Lambda_i+s)$ over the m-th loop in the ACG, P_{m2} are analogous products for the m-th set of two vertex disjoint loops etc. $\Delta_k(s)$ are given also by Eq. (30) with an additional condition that the contributing loops have no vertices in common with the k-th forward path. As all loops in the ACG contain either (μ'), $(\tilde{t}\mu)$ or $(\tilde{p}\mu)$ and all forward paths start at (μ), enumeration of the vertex-disjoint sets is not a formidable task and solutions (29) can be written down rather easily. Additionally, for the solutions for the exit vertices the number of the contributing loops is further reduced. Let us also remark that if only $(\mu') \to (\mu)$ feedback is left, all $\Delta_k(s) \equiv 1$, as there are no loops vertex-disjoint with any of the forward paths.

Similarly to Eq. (20) the total (AC) yields of signatures (17) are now:

$$Y_l^{(AC)} = \lambda_l^{reg} \sum_{\substack{\text{all f.p.} \\ (\mu)\to(l) \text{ in ACG}}} \frac{g_k(0)\Delta_k(0)}{\Delta(0)}. \tag{31}$$

Correspondingly, the (AC) time distributions: are sums of the inverse Laplace transforms of the terms:

$$\frac{\prod_n (\Lambda_n+s)}{\Delta(s) \prod_{\text{ACG nodes}} (\Lambda_n+s)} \prod_{(k,j)} \lambda_{kj} \tag{32}$$

where (k, j) run over all edges in the forward path and in the corresponding vertex-disjoint loop (or loops) and n over all vertices[6] not included in $\Pi_{(kj)}$. In time variable the resulting expressions read:

$$\frac{dS_l^{(AC)}}{dt} = \lambda_l^{reg} \sum_{i=1}^{n_v} e^{-R_i t} H_i(\{\lambda\}, \{\Lambda\}) \tag{33}$$

where

$$H_i(\{\lambda\}, \{\Lambda\}) = \frac{1}{D_i} \sum_{\substack{\text{ACG-f.p.} \\ (\mu)\to(l), \\ \text{v.d.l.}}} \left(\prod_{(k,j)} \lambda_{kj}\right)\left(\prod_n (\Lambda_n - R_i)\right) \operatorname{sgn}(P_{mr}), \tag{33a}$$

$$D_i = \prod_{\substack{\text{all ACG} \\ \text{nodes} \neq (i)}} (R_j - R_i) \tag{33b}$$

and where R_i are zeros of $\det \hat{A}^{(AC)}(s)$ and $\operatorname{sgn}(P_{mr})$ are the corresponding signs in Eq. (30).

---

[6] Let us remark that the sink vertices need not be included here, as the corresponding equations decouple from the others. The time distributions for the sink vertices are simply sums of $\lambda_{\text{sink},j} N_j(t)$. The same argument applies to the cycle-by-cycle formulae.

3. *Experimentally registered signatures*

Due to limited experimental detection efficiency, only a fraction ε of actual transitions is usually registered. The relevant formulae were derived for a few simple situations in Refs. [13–16]. In what follows we show how registration efficiency can be included in the kinetic formulae in the general case considered above.

Let us construct time distribution (17) of the first registered signature. If the detected transition occurs in the k-th cycle, it means that either it remained unobserved in the preceding $k-1$ cycles or the forward path which led to (l) did not include the "measured" edge.

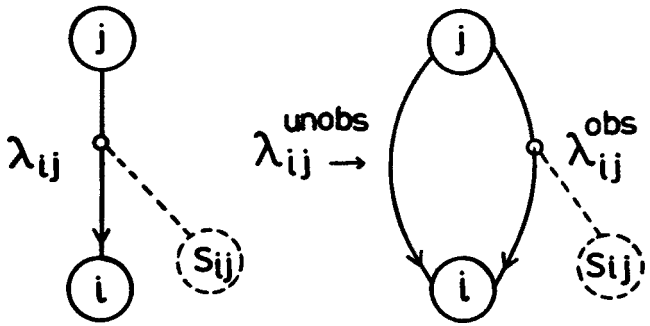

Fig. 7. Inclusion of experimental detection efficiency

This can be easily accounted for by a simple modification of the kinetic graph. Indeed, let us replace the edge corresponding to the measured transition by two parallel links as shown in Fig. 7. Let one of these links represent transitions which are registered ($\lambda_{ij}^{\text{obs}}$), and the other one the transitions which remain unobserved ($\lambda_{ij}^{\text{unobs}}$). The signature vertex is then associated with the "observed" edge. The relative probability for the muon to traverse one of these two edges is determined by the detection efficiency, ε_{ij}, of the signature of the $(j) \to (i)$ transition. Thus

$$\lambda_{ij}^{\text{obs}} = \varepsilon_{ij}\lambda_{ij}, \quad \lambda_{ij}^{\text{unobs}} = (1-\varepsilon_{ij})\lambda_{ij}. \tag{34}$$

According to this picture, the muon that reached the k-th cycle without giving a signal could traverse only the "unobserved" links whenever it went from (j) to (i) in the preceding cycles. Thus, if the first registered transition takes place in the k-th cycle, the time distribution of the associated signatures is given by Eqs. (19) and (16) with the following substitutions:

$$\lambda_l^{\text{reg}} \to \lambda_l^{\text{obs}} = \sum_{\substack{j\text{-measured} \\ \text{transitions}}} \lambda_{jl}^{\text{obs}} = \sum_j \varepsilon_{jl}\lambda_{jl} \tag{35a}$$

in (19), and

$$\lambda_{jl} \to \lambda_{jl}^{\text{unobs}} = (1-\varepsilon_{jl})\lambda_{jl} \tag{35b}$$

in (14) (hence also in $N_i^{(k)}(s)$), and with Λ_i remaining unchanged:

$$\Lambda_i = \sum_j (\lambda_{ji}^{\text{obs}} + \lambda_{ji}^{\text{unobs}}) \to \Lambda_i. \tag{35c}$$

Since the registration may take place in any cycle, the resulting expression (19) has to be summed over all k:

$$s\bar{S}_i^{(1)}(s) = \lambda_i^{\text{obs}} \sum_{k=1}^{\infty} N_i^{(k)}(s; \lambda_{ji} \to \lambda_{ji}^{\text{unobs}}). \tag{36}$$

It is easy to recognize that

$$s\bar{S}_i^{(1)}(s) = \lambda_i^{\text{obs}} N_i^{(\text{AC})}(s; \lambda_{ji} \to \lambda_{ji}^{\text{unobs}}) \tag{37}$$

which follows immediately from Eqs. (26), (32) and (35).

Thus $\bar{S}_i^{(1)}(s)$ is determined by the solution of Eq. (26b) with

$$\hat{A}^{(\text{AC})}(s) \to \hat{A}^{(\text{AC})}(s; \lambda_{ji} \to \lambda_{ji}^{\text{unobs}}). \tag{38}$$

Note that in Eq. (29) for the first registered cycle only $\Delta(s) = \det \hat{A}^{(\text{AC})}$ is affected by substitutions (35b, c). Indeed, $g_m \Delta_m$ correspond here to forward paths which terminate exactly at the vertex for which the solution is sought, thus not including the "measured" edge.

From Eqs. (26) and (38) one can see that analogous formulae for higher registered cycles can be obtained using a straightforward generalization of the presented procedure. Indeed, if an $(l_1) \to (j_1)$ transition is registered at $t = t_1$ the time distributions of signatures which follow are response to a step-function input in the l_1-th node at $t = t_1$. Thus for the subsequent transitions, $(l_2) \to (j_2)$ registered with efficiency $\varepsilon_{j2,l2}$ the corresponding time-distributions will be given again by Eqs. (35)–(38) and (26b) with

$$\vec{I}(s) = \left[0, 0, \ldots \frac{s\phi(s)}{\Lambda_{l_1} + s}, 0, \ldots 0\right]^T \tag{39}$$

with the time variable in Eq. (17) properly shifted. Investigation of such correlated time distributions can be a useful tool in disentangling the complicated kinetic scheme of muon-catalyzed nuclear fusion in mixtures of hydrogen isotopes.

4. Discussion

4.1. Energy-dependent transition rates

In the considerations presented above transition rates were assumed constant. One can envisage, however, that for some objects in the graph transition rates λ_{ij}, in Eq. (1) depend on time which elapses from the moment of their creation, e.g. as a result of degradation of their initial energy. Then in the RHS of Eqs. (1) terms $\lambda_{ij} N_j(t)$ should be replaced by $\int_0^t \lambda_{ij}(t-\tau)\,[dN_j(\tau)/d\tau]d\tau$ which by the convolution theorem leaves unaltered the structure of the equations for the Laplace transformed functions. However, the depend-

ence of the solutions on s may render the description of the kinetics in the time variable prohibitively complicated. Another approximate approach which seems to be more manageable consists in replacing such vertices by sets of nodes corresponding to energy intervals in which the transition rates can be assumed approximately constant. The formalism developed in the previous Sections can be then applied without changes. The only complication is the necessity to deal with an increased number of vertices and, as a result, with a larger number of loops and forward paths. Nevertheless, the complication will amount to replacing the corresponding paths and loops by sets of several ones, and the changes so introduced can be easily controlled.

4.2. Reversible transitions

So far in the derivation of the kinetic formulae we have not included any reversible transitions. In the cycle-by-cycle description this led to Eq. (7) which was the source of simplicity of the formulae that followed. If reversible transitions are admitted, closed loops will appear within OCG. Then, as can be easily seen:

$$\det \hat{A}_1(s) = \det \hat{A}_1^{\mathrm{rev}}(s) = \Delta_1^{\mathrm{rev}}(s), \tag{40}$$

where $\hat{A}_1^{\mathrm{rev}}(s)$ is a submatrix of $\hat{A}_1(s)$ (situated on its diagonal if proper ordering is retained) describing the subset of states between which two-way transitions take place.

Since in a forward path each vertex can be traversed only once at the most, the cycle-by-cycle distributions will be given by equation analogous to (29)

$$N_l^{(k)}(s) = \sum_{\substack{\text{all f.p.} \\ (\mu)_1 \to (l)_k}} \frac{g_m(s)\Delta_m(s)}{[\Delta_1^{\mathrm{rev}}(s)]^k} \tag{41}$$

with the loops describing now the reversible transitions within OCG, which by analogy with Eq. (31) gives immediately the general formula for the total signature yields. The expressions for signature time distributions get slightly more involved in comparison to Eq. (22) where now $\Lambda_j \to R_j$, R_j being zeros of $\Delta_1^{\mathrm{rev}}(s)$ for the vertices in the loops and $R_j = \Lambda_j$ for the other vertices, and the rightmost sum is replaced by

$$\sum_{m=0}^{p-1} \binom{p-1}{m} \left[\sum_{\substack{\{q_1 \dots q_s \dots q_{n_v}\} \\ s \neq j}} (-1)^m \binom{m}{q_1 \dots q_s \dots q_{n_v}} \prod_{\substack{\mathrm{OCG} \\ \text{nodes} \neq (J)}} \frac{(r_n - 1 + q_n)!}{(R_n - R_j)^{r_n + q_n}} \right]$$

$$\times \left\{ \sum_{\substack{\{q_1 \dots q_{n_v}\} \\ q_s \leq \varrho_s}} \binom{p-1-m}{q_1 \dots q_{n_v}} \prod_{\substack{\mathrm{OCG} \\ \text{nodes}}} \left[\frac{\varrho_n!}{(\varrho_n - q_n)!} (\Lambda_n - R_j)^{\varrho_n - q_n} \right] \right\}, \tag{42}$$

where ϱ_n determines the multiplicity of $(\Lambda_n + s)$ in an analogue of Eq. (32). As is seen, although the original simplicity of Eqs. (15)–(22) is to some extent lost, inclusion of

reversible transitions into the kinetic scheme poses no fundamental difficulty and can be accomplished in a straightforward manner.

4.3. Concluding remarks

The presented framework gives a practical tool for the analysis of the experimental data on muon-catalyzed nuclear fusion in arbitrary mixtures of hydrogen isotopes with possible admixtures of heavier elements. Evolution in time of separate cycles in the chain can be described with inclusion of the experimental detection efficiency. Practically any μ-atomic and μ-molecular processes in the chain can be treated strictly in the approximation of constant transition rates. Thus, the formalism provides means to extract from the data the energy-averaged values of the parameters characterizing the muon-catalyzed fusion process, without making additional simplifying assumptions. The topological graph-theoretical approach to construct the kinetic formulae is shown to be particularly useful and simple in application due to a very limited number of the vertex-disjoint loops which can appear in the ACG. It permits also a direct physical interpretation of the terms contributing to the time-distributions of the signatures and, thereby, enables one to control easily the influence of different processes on the kinetics of the chain.

The general character of the presented formulae opens several new possibilities for the experimental investigation of muon-catalyzed nuclear fusion of hydrogen isotopes.

The author is deeply indebted to Prof. L. I. Ponomarev for the stimulating discussions and to Prof. V. P. Dzhelepov for his hospitality at JINR.

REFERENCES

[1] See, e.g., L. I. Ponomarev, *Atomkernenergie/Kerntechnik* **43**, 175 (1983).
[2] S. E. Jones et al., *Phys. Rev. Lett.* **51**, 1757 (1983); *Atomkernenergie/Kerntechnik* **43**, 179 (1983); P. Kammel et al., *Phys. Lett.* **112B**, 319 (1982); J. Zmeskal et al., *Atomkernenergie/Kerntechnik* **43**, 193 (1983); H. Berth et al., *Atomkernenergie/Kerntechnik* **43**, 184 (1983); V. M. Bystritsky et al., *Phys. Lett.* **94B**, 476 (1980); D. V. Balin et al., Preprint LNPI-895, Leningrad 1983. For references to earlier experiments see, e.g., Ref. [20].
[3] E.g., V. M. Bystritsky et al., *Prib. Tekh. Eksp.* **4**, 46 (1984); V. M. Bystritsky et al., *Prib. Tekh. Eksp.* **1**, 46 (1985).
[4] E.g., Yu. V. Petrov, *Nature* **285**, 466 (1980).
[5] S. S. Gershtein et al., *Zh. Eksp. Teor. Fiz.* **78**, 2099 (1980); English transl. *Sov. Phys. JETP* **51**, 1053 (1980).
[6] L. N. Somov, Report JINR P4-81-852, Dubna 1981 (in Russian).
[7] H. Takahashi et al., *Atomkernenergie/Kerntechnik* **36**, 195 (1980).
[8] S. G. Lie, A. A. Harms, *Nucl. Sci. Eng.* **80**, 124 (1982).
[9] A. P. Sguigna, A. A. Harms, *Atomkernenergie/Kerntechnik* **43**, 191 (1983).
[10] A. Kumar, *Atomkernenergie/Kerntechnik* **43**, 203 (1983).
[11] P. Kammel et al., *Atomkernenergie/Kerntechnik* **43**, 195 (1983).
[12] V. M. Bystritsky et al., *Acta Phys. Pol.* **B15**, 699 (1984).
[13] V. V. Filchenkov, L. N. Somov, V. G. Zinov, Preprint JINR E1-83-854, Dubna 1983.
[14] V. M. Bystritsky, A. Guła, J. Woźniak, *Atomkernenergie/Kerntechnik* **45**, 197 (1984).
[15] V. G. Zinov, L. N. Somov, V. V. Filchenkov, Preprint JINR P4-84-45, Dubna 1984 (in Russian).
[16] M. Bubak, V. M. Bystritsky, A. Guła, *Acta Phys. Pol.* **B16**, 575 (1985).

[17] S. S. Gershtein et al., *Zh. Eksp. Teor. Fiz.* **80**, 1690 (1981); L. Bracci, G. Fiorentini, *Nucl. Phys.* **A364**, 383 (1981).
[18] See e.g., S. Seshu, M. B. Reed, *Linear Graphs and Electrical Networks*, Addison-Wesley Publishing Comp., Inc., Reading, London 1981, Chapter 10.
[19] See, e.g., A. Bertin, A. Vitale, A. Placci, *Nuovo Cimento* **5**, 423 (1975) and references quoted therein.
[20] See, e.g., L. I. Ponomarev, in Proc. of 6-th Int. Conf. on Atomic Physics, Riga 1978, Zinatne, Riga; Plenum Press, New York and London 1978, p. 182.
[21] D. D. Bakalov, V. S. Melezhnik, S. I. Vinitsky, *Zh. Eksp. Teor. Fiz.* **79**, 1629 (1980); English transl. *Sov. Phys. JETP* **52**, 5 (1980).
[22] S. J. Mason, *Proc. Inst. Radio Engrs.* **44**, 920 (1956) (see also Ref. [18]).
[23] L. N. Bogdanova, V. E. Markushin, V. S. Melezhnik, L. I. Ponomarev, *Yad. Fiz.* **34**, 1191 (1981); English transl. *Sov. J. Nucl. Phys.* **34**, 662 (1981); L. N. Bogdanova, V. E. Markushin, V. S. Melezhik, L. I. Ponomarev, *Zh. Eksp. Teor. Fiz.* **81**, 829 (1981); English transl. *Sov. Phys. JETP* **54**, 442 (1981).
[24] H. Takahashi, A. Moats, *Atomkernenergie/Kerntechnik* **43**, 188 (1983); V. P. S. Tan, *Nature* **263**, 656 (1976).